M.E. Weber and T.A. Noyes

Wind Shear Detection with Airport Surveillance Radars

Airport surveillance radars (ASR) utilize a broad, cosecant-squared elevation beam pattern, rapid azimuthal antenna scanning, and coherent pulsed-Doppler processing to detect and track approaching and departing aircraft. These radars, because of location, rapid scan rate, and direct air traffic control (ATC) data link, can also provide flight controllers with timely information on weather conditions that are hazardous to aircraft. With an added processing channel, an upgraded ASR can automatically detect regions of low-altitude wind shear. This upgrade can provide wind shear warnings at airports where low traffic volume or infrequent thunderstorm activity precludes the deployment of a dedicated Terminal Doppler Weather Radar (TDWR). Field measurements and analysis conducted by Lincoln Laboratory indicate that the principal technical challenges for low-altitude wind shear detection with an ASR—ground-clutter suppression, estimation of near-surface radial velocity, and automatic wind shear hazard recognition—can be successfully met for microbursts accompanied by rain at the surface.

This article describes radar modifications and processing techniques that allow airport surveillance radars (ASR) to detect microburst-generated low-altitude wind shear. Microbursts have been identified as the primary cause of 12 major air carrier accidents since 1970, resulting in the loss of 575 lives. For airports with low traffic density or infrequent thunderstorm activity, an upgrade to ASRs provides wind shear warnings at a lower cost than that of dedicated wind shear detection sensors.

Modern digital signal processing for the newest ASRs—the ASR-9s—generally eliminates clutter from precipitation and ground scatterers [1, 2]. Early acceptance testing of the ASR-9, however, indicated that working air traffic controllers actually made considerable use of the weather-echo information on their displays. To reinsert weather data in a noninterfering manner, the ASR-9's signal processor was augmented with a dedicated channel for processing and displaying six quantitative levels of precipitation reflectivity (i.e., rain rate) [2, 3]. This processor does not utilize the radar's coherence, other than for Doppler filtering of stationary ground-clutter echoes.

Techniques to extend the ASR's weather measurement capability to allow for the detection of thunderstorm-generated low-altitude wind shear must incorporate (*a*) signal processing for suppressing ground clutter and estimating the near-surface radial wind component in each radar resolution cell, and (*b*) image processsing for automatically detecting hazardous shear in the resulting velocity field.

Algorithms that accomplish these functions have been evaluated extensively with simulated weather signals and measurements from an experimental ASR in Huntsville, Ala. Our analysis indicates that a suitably modified ASR could with high confidence detect microbursts accompanied by rain at the surface—the predominant safety hazard for aircraft in many parts of the United States. The following section describes the background and potential operational role of an ASR-based wind shear detection system. We then discuss the primary technical issues for achieving this capability, and describe our evaluation of processing methods that address these issues.

Background and Operational Mission

Figure 1 illustrates the two principal causes of low-altitude wind shear. In Fig. 1(a), an intense thunderstorm downdraft encounters the earth's surface and produces a brief outburst of highly divergent horizontal winds, or microburst [4]. Aircraft that penetrate a microburst on takeoff or landing experience head-wind-to-tail-wind velocity shear compounded by a downdraft in the microburst core. Gust fronts are thunderstorm outflows whose leading edges propagate away from the generating precipitation, as shown in Fig. 1(b) [5]. Because the wind shear encountered by an aircraft that penetrates a gust front increases the plane's lift, a gust front is considered less hazardous than the wind shear associated with a microburst. The winds behind the gust front, however, are turbulent, and the long-term change of wind direction following the passage of a gust front affects runway operations. Tracking and predicting gust front arrivals at major airports

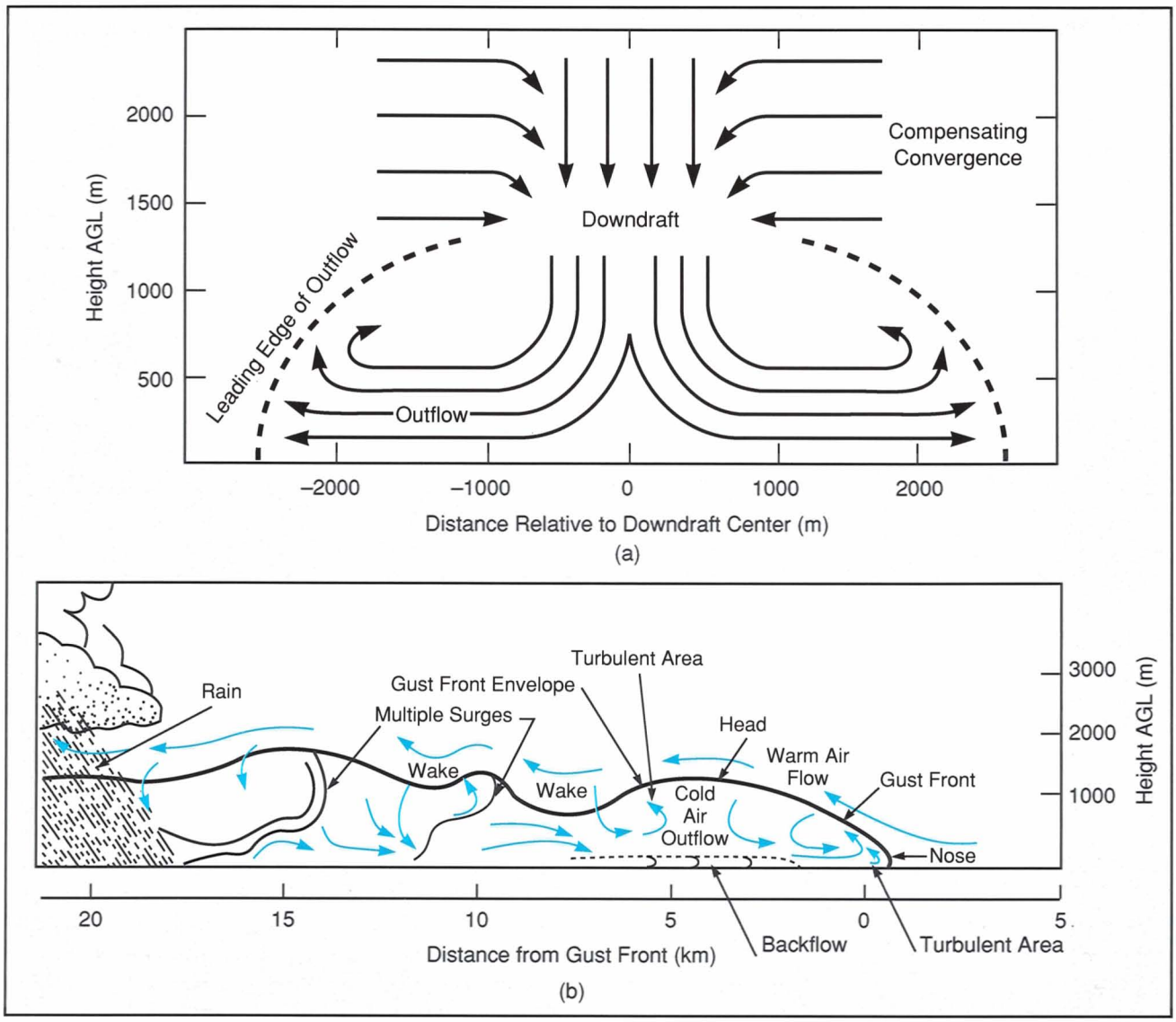

Fig. 1—(a) Vertical cross section of microburst wind field. (b) Vertical cross section of gust front (redrawn from Goff, Ref. 5).

will allow more efficient use of runways.

In response to the hazards of wind shear, the Federal Aviation Administration (FAA) initiated a two-part enhancement to its terminal-area weather information system. The airport network of surface wind-speed and wind-direction sensors—the Low Level Wind Shear Alert System (LLWAS)—is being improved by a reworked detection algorithm and, at major airports, an increased number of sensors [6]. In addition, a dedicated microwave Terminal Doppler Weather Radar (TDWR) will be deployed at 45 airports to measure the radar-reflectivity and radial-velocity signatures associated with low-altitude wind shear [7].

ASRs were initially rejected as candidate wind shear detection sensors because of their perceived deficiencies in sensitivity and ground-clutter rejection, as well as an inability to resolve near-surface thunderstorm outflows with the broad elevation beams. To the extent that these problems can be overcome, however, ASR-9s will complement the dedicated wind shear detection sensors in three areas:

(1) Airports with low traffic volume or in regions with infrequent thunderstorm activity may not warrant a dedicated TDWR or enhanced LLWAS. A modified ASR could provide wind shear protection at these airports at a smaller cost than the dedicated systems.

(2) At airports equipped with enhanced LLWAS but lacking TDWR, data from an ASR could reinforce LLWAS wind shear reports and detect wind shear in operationally significant areas not covered by the surface station network.

(3) At airports slated to receive a TDWR, additional radar wind measurements from an ASR could help to reduce head-wind–tail-wind shear-estimate inaccuracies that result when a microburst outflow is asymmetric. The siting of the ASR will often provide a better viewing angle than the TDWR for head-wind–tail-wind shear measurements along some runways. Alternately, data from the two radars may be combined to compute the total horizontal component of the wind vector over areas where radials from the two radars intersect at approximately right angles. In addition, the rapid scan rate of an ASR (12.5 scans/min) would provide more frequent updates on wind shear than are currently planned in the TDWR scanning strategy.

The FAA has sponsored the Air Traffic Surveillance Group at Lincoln Laboratory to investigate the ASR-9's wind shear detection capability and develop the above benefits. Initial work used data from meteorological Doppler radars and operational ASRs to develop candidate signal processing sequences and analyze their expected performance [8, 9]. Results of these analyses led to the deployment in 1986 of an experimental ASR-8 near Huntsville, Ala. Lincoln Laboratory modified the radar transmitter to provide better stability and the capability to transmit either a constant pulse-repetition frequency (PRF) waveform or the alternating PRF sequence used by the ASR-9. A time-series data-acquisition system allowed for simultaneous recording of in-phase and quadrature signals out to a maximum instrumented range of 60 nmi. This broadband recording capability has facilitated comparative evaluation of various signal processing techniques. A pencil-beam Doppler weather radar was colocated with the ASR to provide three-dimensional radial wind measurements for comparison with the ASR estimates.

Interference Rejection and Estimation of Low-Altitude Velocity

Table 1 outlines parameters of the ASR-9. Vertically displaced feedhorns produce two antenna patterns, shifted in elevation angle by 3.5°. The aircraft-detection channel utilizes the higher beam at short range to reduce ground clutter, and switches to the low beam beyond about 10 nmi. While the transmitted power, operating frequency, and receiver parameters are well suited to weather sensing, the radar's broad elevation beam patterns and rapid azimuthal antenna scanning produce significant challenges for wind shear

Table 1. ASR-9 Parameters

Transmitter	
Frequency	2.7-2.9 GHz
Polarization	Linear or Circular
Peak Power	1.1 MW
Pulse Width	1.0 μs
Block-Staggered CPI Lengths	8 pulses/10 pulses
PRFs (Example)	972 s^{-1}/1250 s^{-1}
Receiver	
Noise Figure	4.1 dB (max)
Sensitivity	–108 dBm
A/D Word Size	12 bit
Antenna	
Elevation Beamwidth	4.8° (min)
Azimuth Beamwidth	1.4°
Power Gain	34 dB
Rotation Rate	12.5 RPM

detection as described below.

One difficulty with an ASR is its limited capability for measuring wind shear events with low radar cross-section densities. The reflectivity density of meteorological targets is normally expressed in terms of the *radar reflectivity factor*. The reflectivity factor for clear-air scatterers such as insects or refractive index inhomogeneities is 10 dBz or less. Mist or light rain return echoes of 20 to 30 dBz, while maximum reflectivities in severe thunderstorms can exceed 70 dBz. Because microbursts in most parts of the country occur in association with heavy rain, at least part of the outflow wind region has high radar reflectivity. In the high plains of the United States, however, *dry* microbursts may occur when rain falls through a deep, dry subcloud layer before reaching the ground. Reflectivity values associated with these microbursts range from 0 to 30 dBz. Gust fronts can also be associated with low reflectivity factors, since the leading edge of the strong winds can move rapidly away from the generating precipitation.

Current ASRs employ range-dependent sensitivity time control (STC) to prevent large targets such as ground clutter from saturating the receiver or A/D converters at short range. The limit for detection of low-reflectivity thunderstorm outflows is therefore a function of the chosen STC setting, as well as the radar transmitter, antenna, and receiver characteristics. Figure 2 plots the minimum detectable weather reflectivity factor (assuming 0-dB SNR requirement) versus range for an ASR-9. The calculation assumes STC attenuation that varies as the inverse square of range, with a cutoff at 23 km. We have shown that, for representative ground-clutter environments, this setting provides acceptable sensitivity while minimizing system saturation caused by the clutter [10]. The curves also include beamfilling loss to account for the portion of the transmitted energy that does not

intercept shallow near-surface thunderstorm outflows. The different curves are for high (dashed) and low (solid) receiving beams, assuming outflow depths of 300 m or 500 m. Such values are representative of the depth of microburst outflows [11].

Given the on-airport location of ASRs, microburst detection is operationally relevant only in the range interval of 0 to 12 km. Throughout this area of detection, microburst outflows with reflectivity factors greater than approximately 10 dBz will be measurable with the low receiving beam. The sensitivity of the high receiving beam, if it uses the same STC function, is approximately 10 dB poorer at 12-km range, due to greater beamfilling loss. We conclude that, in environments such as the high plains, inadequate sensitivity could prevent an ASR from detecting some microbursts that are not accompanied by rain at the surface. However, for the large areas of the United States where essentially all microbursts occur in heavy rain, an ASR's sensitivity will be sufficient for microburst detection.

Gust front echoes frequently extend higher than 500 m. Thus beamfilling loss will be less than the calculated values shown in Fig. 2. An

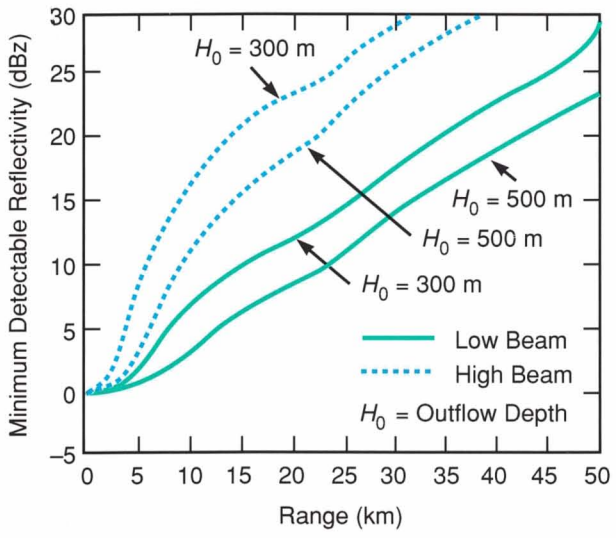

Fig. 2—ASR-9 system noise level expressed in terms of the equivalent weather reflectivity factor. Beamfilling losses for a 300-m or 500-m deep thunderstorm outflow are included.

ASR can measure gust fronts with reflectivity factors greater than 15 dBz out to a range of 30 km; this capability provides an airport with useful forecasts of wind shifts. A significant fraction of gust fronts, however, exhibit maximum reflectivity factors less than the above value and are not detectable from ASR measurements. Since the operational benefits associated with gust front detection occur primarily at major airports—airports that will be equipped with a TDWR—the less reliable gust front detection capability of an ASR is not viewed as critical.

Sensitivity considerations, along with the need to maximize power received from near-surface outflow layers relative to scatterers aloft, dictate that the low receiving beam of an ASR be used for wind shear detection, even at short range. Signals in the low beam are contaminated with intense ground clutter at short range. Ground-clutter measurements from the ASR in Huntsville were analyzed to quantify the performance of a specific clutter-suppression scheme [9]. A bank of finite impulse response (FIR) high-pass filters was used to allow adaptive selection of one of the filter transfer functions based on the intensity of clutter and weather in each resolution cell. This procedure minimizes distortion of the weather-echo spectrum in the filtering process. The clutter filters operate coherently across the PRF transitions of the ASR-9's waveform [8].

Figure 3 illustrates the conclusions derived from the analysis. Here, signals from a simulated microburst were combined with the measured ground-clutter distribution to map out areas where the wind shear signature could be successfully extracted from clutter. The simulation took into account the stochastic nature of echoes from ground clutter as well as the prescribed signal processing approach. The area obscured by ground clutter is plotted, assuming microburst reflectivity factors varying from 10 to 30 dBz. When the reflectivity factor exceeds 20 dBz, areas of clutter-induced obscuration are fragmented so that a microburst signature is recognizable over at least part of its aerial extent. Conversely, recognition of low-reflectivity microbursts or gust fronts (<<20 dBz) at

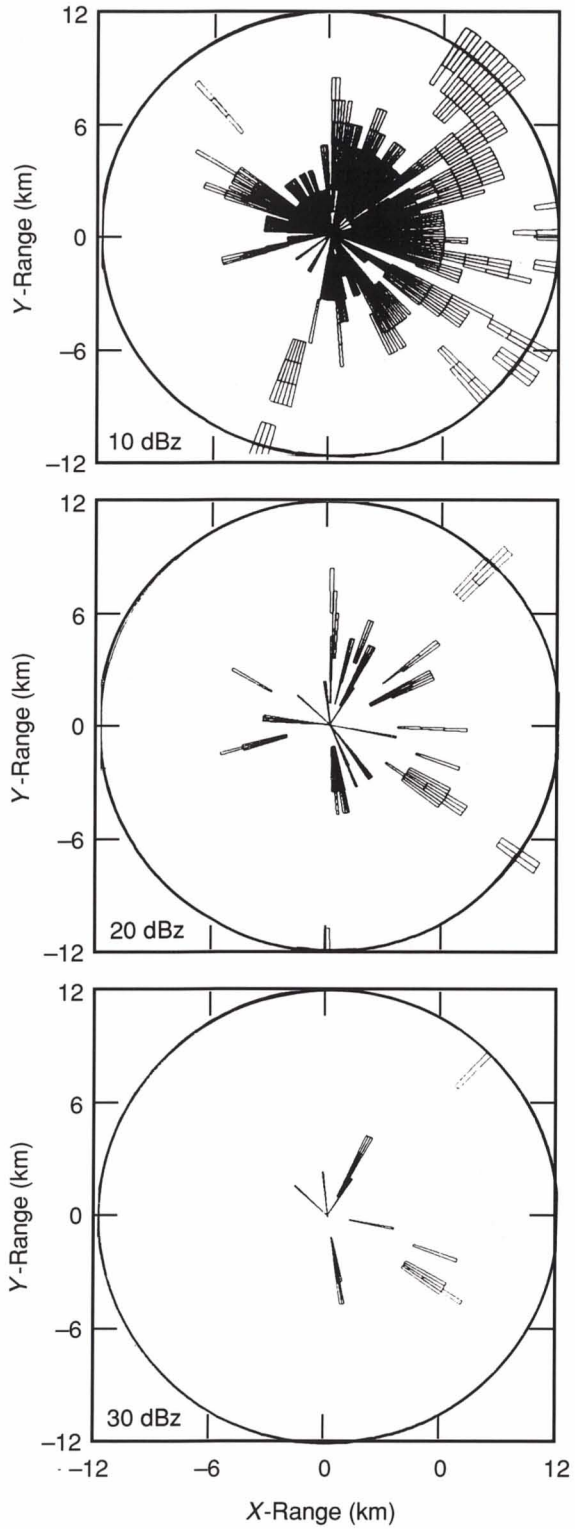

Fig. 3—Calculated area of obscuration for a microburst at our radar site at Huntsville, Ala. Weather reflectivity factors of 10, 20 and 30 dBz are assumed.

ranges less than 6 km may be difficult because of ground-clutter residue.

A third problem for accurate low-altitude velocity measurement with an ASR results when energy is scattered into the elevation fan beam from precipitation above shallow microburst outflows. This overhanging precipitation normally has a radial velocity markedly different from the radial velocity in the outflow layer. As a result, the power spectrum of the echo received by an ASR is broad and asymmetric, which reflects contributions from various altitudes with different radial velocities. The power-weighted mean Doppler velocity—the conventional weather-radar radial wind estimator—will thus be intermediate between the outflow velocity and winds aloft.

Figure 4 shows velocity spectra measured with the testbed ASR at the point of strongest outflow winds in Huntsville microbursts. Both high- and low-beam spectra are displayed. The plots in the left column illustrate the approaching (negative) velocity core and those in the right column illustrate the corresponding receding (positive) velocity core. The spectra have been normalized to have the same integrated area. For reference, low-elevation-angle (0.7°) mean radial velocities measured at the same locations and times with the colocated pencil-beam Doppler weather radar are indicated by dashed vertical lines.

Relative to the pencil-beam measurements, these spectra show significant rms width (2 to 10 m/s) due to the elevation beam pattern of the ASR and the strong vertical shear in the wind field above microbursts. If a power-weighted mean-velocity estimator is used with the ASR signals, the estimates would differ significantly from the pencil-beam radar measurement, and wind shear as measured by the ASR would be underestimated. The underestimate is greater for the high beam than the low beam, and generally increases with range.

Signal processing techniques to overcome this problem separate spectral components associated with low elevation angles from those produced by winds aloft. This separation is

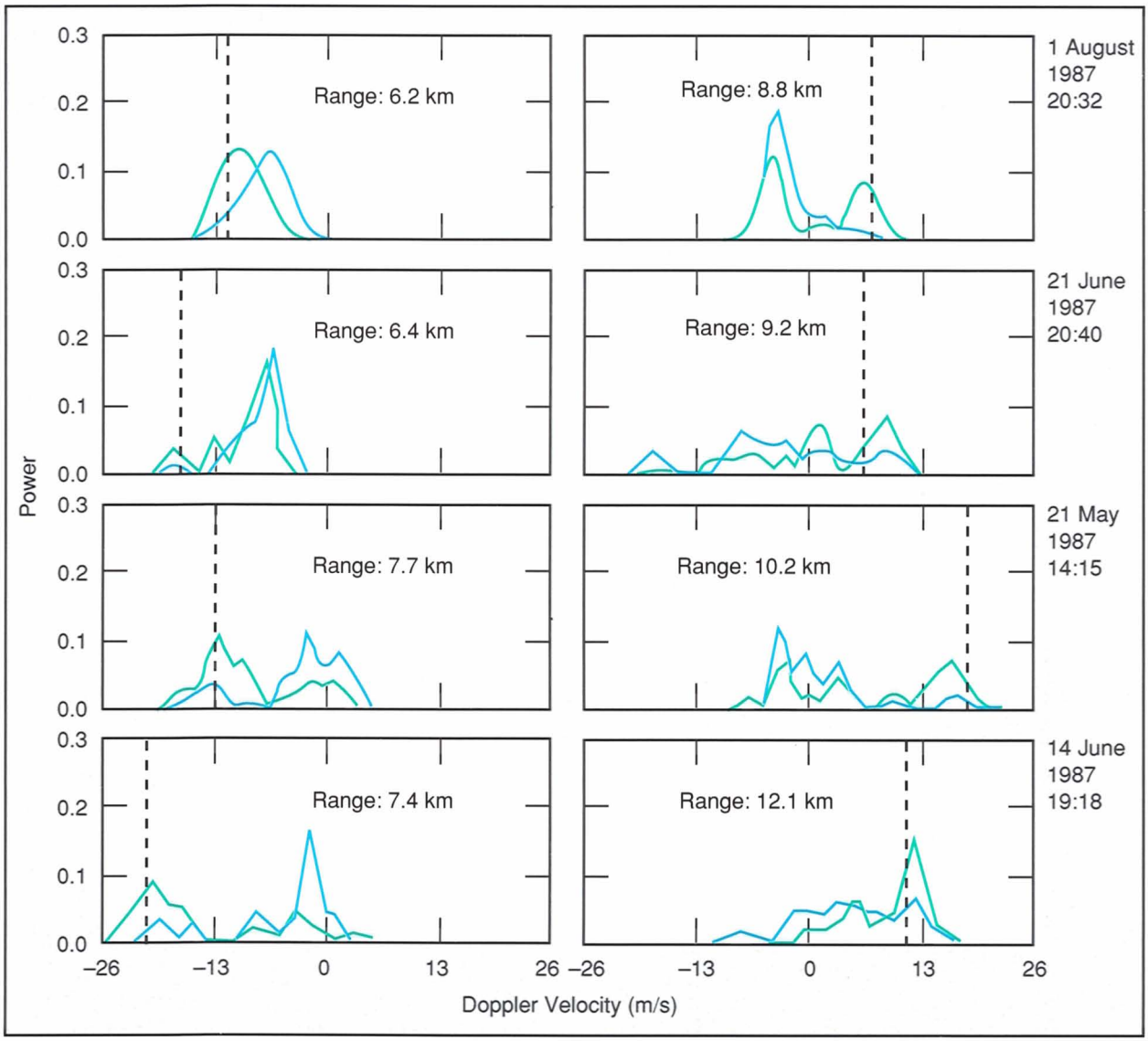

Fig. 4—Examples of power spectra measured with an ASR in approaching (left) and receding (right) microburst radial-velocity cores. The ordinate is relative power in linear units. Green and blue curves illustrate low and high receiving beams, respectively. The dashed vertical lines show the radial velocity measured by the pencil-beam radar at 0.7° elevation angle at the same locations and times.

accomplished by comparing the amplitude and/or phase of signals received in the low receiving beam with those in the high beam. Figure 5 shows that low- and high-beam amplitude patterns for an ASR differ significantly at elevation angles below 5° with the difference increasing monotonically toward the horizon. In addition, the vertically displaced feedhorns produce an interferometric phase difference between signals in the two channels; this phase difference varies approximately linearly with elevation for small elevation angles.

Comparison of the measured power spectra in Fig. 4 with the antenna gain patterns in Fig. 5 immediately suggests one method for discriminating between signal components from low and high elevation angles. As would be expected, the power spectrum density (PSD) of low-beam signals significantly exceeds that of high-beam signals for velocity components near

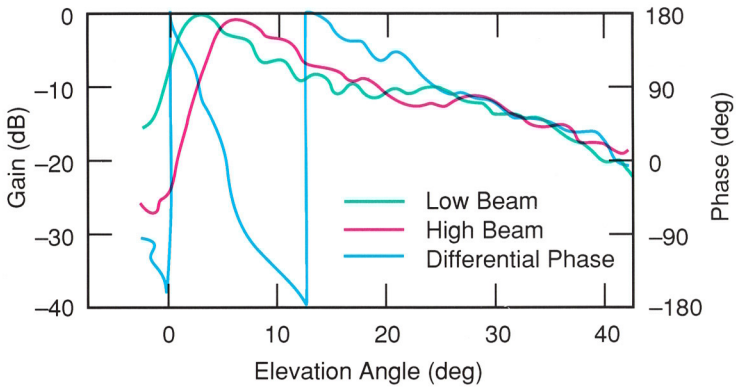

Fig. 5—Elevation amplitude and differential phase patterns of ASR-9 antenna.

the measured near-surface mean radial velocity. One algorithm for exploiting this systematic relationship between high- and low-beam PSDs in microbursts involves (*a*) transforming high- and low-beam signals into the frequency domain, followed by incoherent averaging in range, azimuth, and time to generate acceptably stable PSD estimates; (*b*) subtracting the high-beam

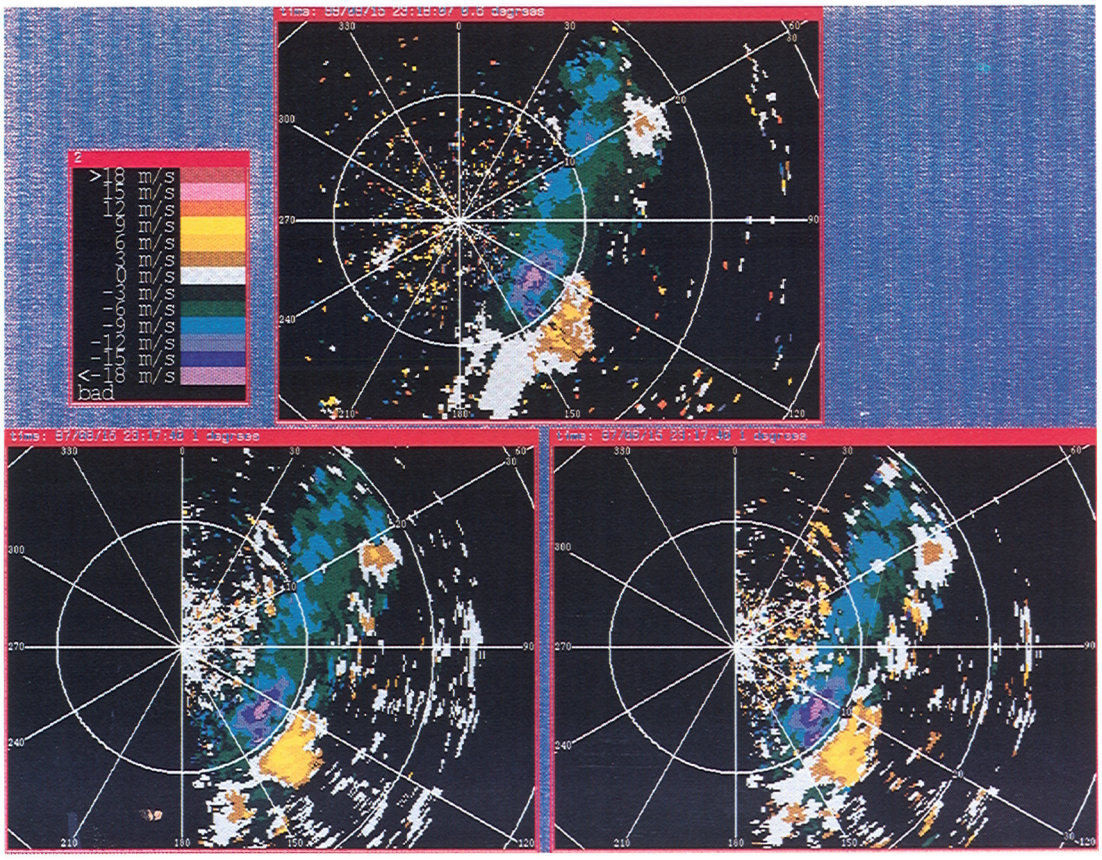

Fig. 6—Radial-velocity fields in a microburst-producing thunderstorm. Upper panel shows measurements from the pencil-beam radar scanning at 0.7° elevation angle. The lower left and right panels show ASR estimates that use, respectively, the autocorrelation-based and spectral-differencing techniques described in the text. Negative velocities (blues and greens) indicate winds with a component toward the radar.

PSD from the low-beam PSD; (*c*) identifying that positive lobe in the difference spectrum with the greatest integrated power; (*d*) calculating the power-weighted mean of this lobe [12, 13].

An analogous procedure eliminates the computationally expensive time-frequency transformation required above [14]. Consistent with many of the measured spectra, the power spectrum of ASR weather signals is modeled as a summation of two Gaussian-shaped components with unknown amplitude, center frequency, and width. Solutions for these parameters can be obtained from measurements of low-order lags of the low- and high-beam signal autocorrelation functions. The center frequency of the low-altitude Gaussian spectrum component gives the desired near-surface radial-velocity estimate.

Figure 6 compares radial-velocity fields estimated from the signals from our experimental ASR with radial-velocity fields measured by the pencil-beam weather radar. Data are from a microburst-producing thunderstorm in Huntsville on 15 August 1988. The upper panel is the pencil-beam radar's measurement from a scan at 0.7° elevation angle. Two microbursts were present, a strong outflow centered at 10 km range/130° azimuth and a weaker event at 15 km/65°. ASR estimates using the low/high-beam spectral-differencing technique are shown in the lower right panel with the corresponding autocorrelation-based estimate in the lower left panel. The velocity fields derived from the ASR signals agree well with the velocity fields measured by the weather radar. In particular the measurements clearly indicate the presence of the two microbursts, and the ASR velocity-differential estimates across the microbursts are within 1 m/s of the pencil-beam measurements.

Anderson proposed that the elevation-angle-dependent phase difference between high- and low-beam signals could be exploited to determine the height associated with each measured spectrum component in received signals from an ASR [15]. The complex cross-spectral density of high- and low-beam signals provides the appropriate frequency-resolved phase measure. Figure 4 shows that the high/low-beam differential phase is single-valued for the elevation domain from 2.5° below to 11° above the nose of the low beam. Examination of the antenna gain patterns suggests that ambiguities at higher angles can be resolved up to about 20° by comparing low- and high-beam power spectrum densities.

Automatic Recognition of Hazardous Velocity Divergence

An algorithm for computer recognition of hazardous divergence in a single-Doppler radial-velocity field is described by Merritt et al. [7]. The Microburst Divergent Outflow Algorithm (MDOA) initially searches along radials to identify segments of monotonically increasing velocity that correspond to a headwind loss for a penetrating aircraft. These segments are grouped by azimuth and then subjected to loose temporal-continuity requirements before declaring a microburst alarm.

Initial end-to-end testing of ASR-based microburst detection applied the MDOA to radial-velocity fields that were estimated as in the preceding discussion. To reduce off-line data processing time, our evaluation sparsely sampled the available data from the experimental ASR. Typically only one or two of the 12.5 scans/min were passed through the data processing sequence of clutter filtering, low-altitude velocity estimation, and automatic microburst recognition. Alarms from the detection algorithm were then scored by a simple hit-miss criterion with respect to microburst locations determined from the pencil-beam weather-radar data.

Table 2 summarizes the scoring results on a scan-by-scan basis for two years of data collected in Huntsville. The spectral differencing method described above was used for velocity estimation. Only microbursts centered within the operationally significant region extending 12 km from the radar were scored. The listed performance metrics are

(1) probability of detection—the number of detected microburst signatures divided by the total number of microburst signatures;

Table 2. Microburst Detection Algorithm Performance for ASR-Based Velocity Fields (Low-High Beam Spectral Differencing)

1987 Data			
	ΔV_R > 10 m/s	ΔV_R > 15 m/s	ΔV_R > 20 m/s
Detection Probability	0.92	0.96	1.00
False Alarm Probability	0.04	0.01	0.02
ΔV_R Bias (m/s)	–1.8	–2.7	–3.0
RMS ΔV_R Discrepancy (m/s)	4.6	5.0	5.4
1988 Data			
	ΔV_R > 10 m/s	ΔV_R > 15 m/s	ΔV_R > 20 m/s
Detection Probability	0.93	0.93	0.97
False Alarm Probability	0.02	0.02	0.0
ΔV_R Bias (m/s)	0.4	–1.0	–1.0
RMS ΔV_R Discrepancy (m/s)	3.4	3.2	3.4

(2) probability of false alarm—the number of algorithm alarms not associated with microbursts divided by the total number of alarms;
(3) bias—the average difference between ASR-based and pencil-beam-radar microburst differential-velocity estimates; and
(4) rms difference between the pencil-beam radar and ASR-based velocity-differential estimates.

These metrics are tabulated separately for all microbursts and for the subsets of more operationally significant microbursts with differential velocities greater than 15 and 20 m/s. The events considered, as with almost all Huntsville microbursts, were characterized by high radar reflectivity.

These statistics indicate a very useful wet-microburst detection capability for a modified ASR. Detection and false-alarm probabilities are uniformly within the 0.9/0.1 limits of the FAA's TDWR System Requirements Statement. Estimates of radial-velocity divergence in the detected microbursts differ on average by 3 to 5 m/s from the closest (in time) available measurements with the pencil-beam weather radar. Similar results apply to detection-algorithm performance using the autocorrelation-based ASR velocity estimates [14] and the coherent cross-spectral velocity estimator [15].

We are currently evaluating the extent to which the rapid scan rate of an ASR can be exploited in the microburst detection process. Potential benefits include more timely first detection, better tracking of events that are growing rapidly or whose centroid is moving, and improved delineation of the hazard region through temporal stabilization of computed divergence regions.

A divergence-based algorithm (DBA) designed to take advantage of the scan rate of an ASR is under evaluation. Pointwise radial-velocity divergence is estimated directly from the velocity field; hazard regions are then determined by thresholding the resulting divergence

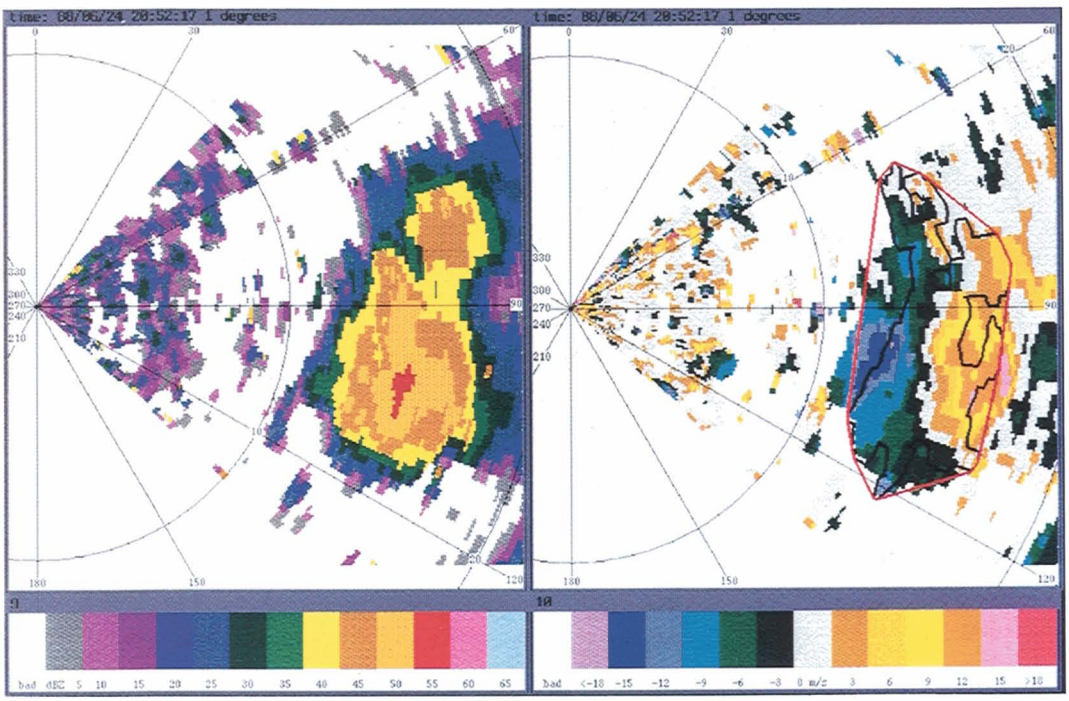

Fig. 7—Reflectivity field (left) and radial-velocity field (right) measured by the experimental ASR in a microburst-producing thunderstorm. The black region in the radial-velocity field shows the area of strong divergence detected by the image-processing algorithm described in the text. The red convex hull for this region provides a simpler representation of the hazard for air traffic control applications.

field. The divergence estimate is the slope of a least-squares linear fit to velocity measurements in a radial window surrounding each resolution cell. This window is relatively broad to filter out small-scale perturbations in the wind field.

Divergence estimates may be unstable from scan to scan. The rapid rotation rate of an ASR allows us to apply time-continuity constraints to the thresholded divergence field. The algorithm increases either a positive or a negative map at each point on successive scans, depending on whether a divergence threshold was or was not exceeded. When a cell in the positive map is incremented, the corresponding cell in the inverse map is zeroed. If the positive map value exceeds a preset threshold in a resolution cell (corresponding typically to detection on two successive scans), that cell is included in the formation of shear regions. Conversely, negative map values greater than a second threshold (indicating lack of strong divergence on a specified number of consecutive scans) cause the associated positive map cell to be zeroed, thereby excluding that cell from any shear region.

Two-dimensional shear regions are formed with the positive map as input. Those resolution cells exhibiting temporally stable strong divergence are delineated by using a directed boundary walk. The boundary walk creates eight-connected [16] regions. Regions smaller than a specified area are eliminated to reduce anomalies while retaining true microburst regions.

The resulting regions frequently exhibit complex spatial structure. To allow for easy interpretation, the minimum bounding convex polygon, or convex hull [17], is computed as the final output product. Intersections between this shape and runway approach or departure corridors will result in issuance of microburst alerts to aircraft.

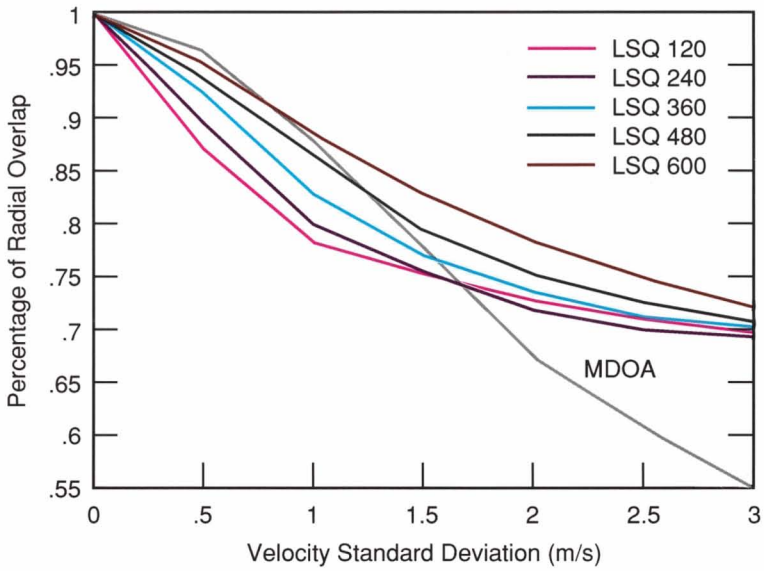

Fig. 8—Calculation of the effectiveness of radial-shear detection in TDWR MDOA and ASR divergence-based algorithms. The average percentage of length detected for a simulated divergence is plotted versus rms velocity estimate error. The gray curve represents the MDOA estimate and the other curves represent least-squares divergence-based estimates with varying radial-window size.

Figure 7 superimposes the shear region found by the DBA on a radial-velocity field estimated from our experimental ASR. The black outline shows the region of strong divergence and the simpler red shape depicts the associated convex hull. The outlines accurately bound the area where an airplane would encounter significant headwind loss. In this case the storm was moving rapidly from north to south. As a result of the temporal filtering logic of the algorithm, the declared hazard region extends northward slightly beyond the region of strong divergence.

Simulated data were used to compare the effectiveness of the radial-divergence detection phase of the TDWR MDOA with that of the DBA. The one-dimensional radial-velocity variation in a microburst was modeled as the positive-slope portion of a sine wave. Gaussian noise was added at each point along the curve to simulate the statistical uncertainties in velocity estimates from fluctuating weather echoes.

Algorithm performance was quantified by using the percentage of radial overlap of the estimated divergence with that portion of the sine wave exhibiting divergence in excess of 2.5×10^{-3} s^{-1}. At this threshold, divergence is considered operationally hazardous to aircraft.

Figure 8 shows the relationship between the percentage of radial overlap and velocity standard deviation for the MDOA and for the DBA with least-squares filter radii ranging from 120 to 600 m. Performance statistics were obtained by applying the algorithms over 1,500 trials, or radials. The length and the strength of the hazard signature were fixed at 4 km and 10 m/s, respectively, which simulates a microburst of minimum severity. Velocity-estimate rms error was varied from 0 to 3 m/s.

For all methods, the average percentage of hazard length detected decreases as the velocity-estimate error increases. For rms velocity errors less than 1 m/s, the MDOA results in a higher percentage overlap than the divergence-based method; the converse applies at high-velocity errors. Coherent integration periods for TDWR have been set so that the velocity-estimate standard deviation is less than 1 m/s. For

a fast-scanning ASR, however, estimate errors may sometimes be as large as 2 to 3 m/s, even after spatial filtering [14]. Thus the divergence-based approach may be a more suitable match to the characteristics of velocity fields estimated from ASR signals.

Figure 8 also shows that the performance of the divergence-based method increases as the radius of the least-squares fit increases. Practically, however, the least-squares window can become too large in relation to the microburst size. In the case shown, where the length of the signature is 4 km, we have found 1 km to be the maximum effective window size. To detect all microbursts, which can be as small as 800 m in diameter [18], we have chosen 400 m as a practical window radius.

Based on our evaluation to date, we are confident that computational speed, simple logic, and accuracy in depicting the actual regions of strong divergence make the divergence-based algorithm appropriate for use with an ASR.

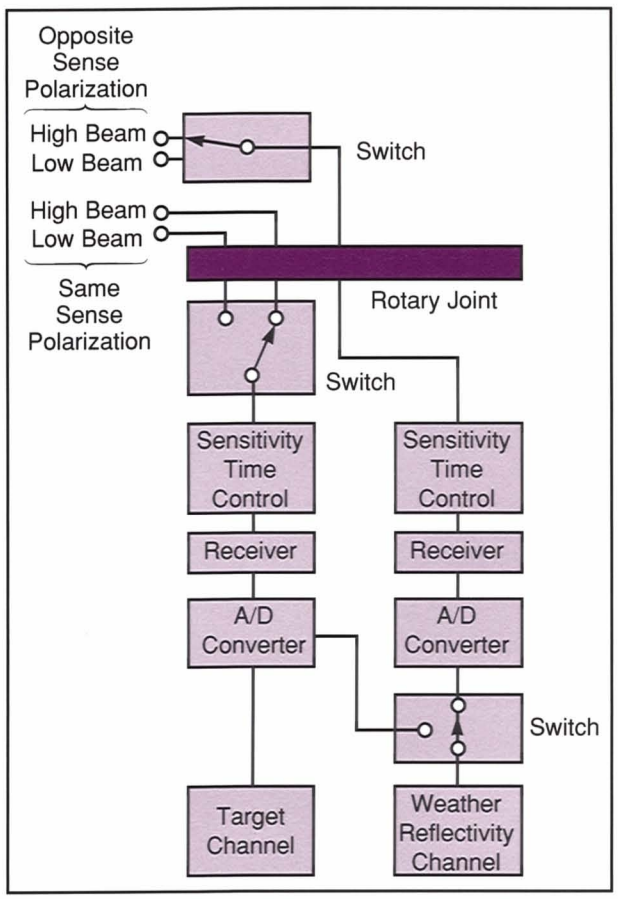

Fig. 9—Simplified diagram of existing signal paths from ASR-9 antenna to airplane target processor and existing weather reflectivity processor.

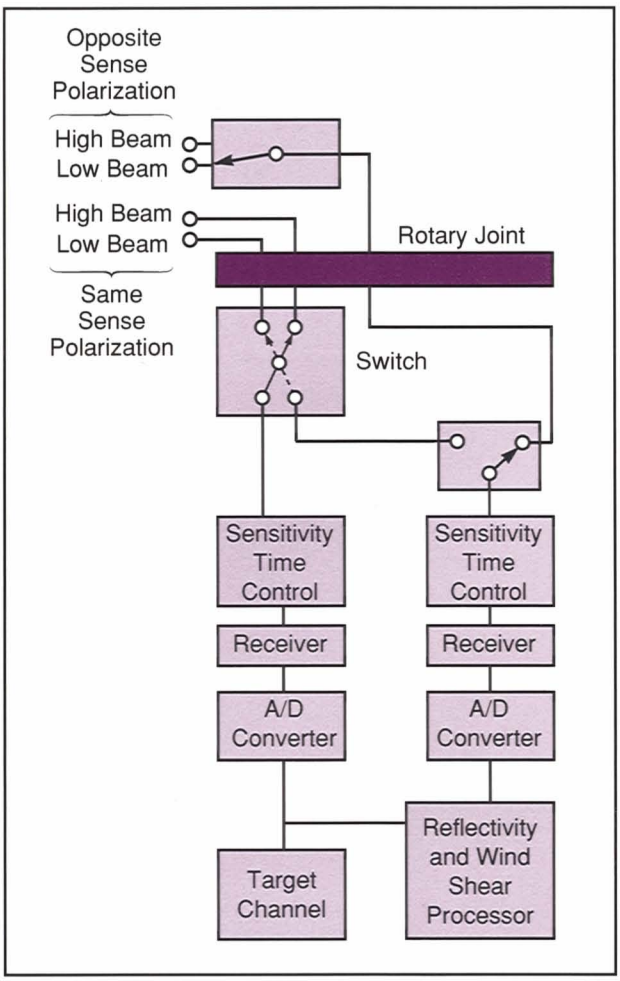

Fig. 10—Diagram of modified ASR-9 signal path configuration to allow for low-altitude wind shear processing.

Required Radar Modifications

Our testbed ASR was designed to permit the collection of signals in modes that an operational ASR-9 would not support. Capabilities such as access to low-beam data at short range, the ability to utilize an STC function that would not obscure low-reflectivity wind shear events, and the simultaneous availability of low- and high-beam signals would require the insertion of signal paths, receivers, and processing equip-

ment not currently in ASRs. As shown in this section, these capabilities can be added without affecting the radar's primary mission of aircraft detection and tracking.

Figure 9 is a schematic diagram of the current signal paths in an ASR-9, from the antenna to the A/D converters. When the radar transmits linearly polarized (LP) signals, both the aircraft detection processor and the six-level weather-reflectivity channel receive signals from the same-sense polarization ports on the antenna feeds. Both high- and low-beam signals are brought through the rotary joint in waveguide, and a single set of A/D converters are switched between the beams in a range-azimuth gated (RAG) mode. When the radar transmits circularly polarized (CP) signals, the target channel continues to receive same-sense polarized data while weather processing is accomplished by using unattenuated weather signals from the orthogonal-sense antenna ports. Only one RF path through the rotary joint is available for the opposite-sense signals, so RAG switching between the high and low beams must be accomplished on the antenna.

Figure 10 shows modifications to these paths that allow the acquisition of low- and high-beam signals at short range as required for wind shear detection. For LP operations, the single-pole, double-throw switch between the high and low beams is replaced by a double-pole, double-throw switch. This modification shunts low-beam signals to the combined reflectivity and wind shear processor for the range interval over which the target channel employs high-beam signals. A separate STC module, receiver, and A/D converter pair are installed for this path. High-beam data are simultaneously available to the weather processor from the target-channel A/D converters. If the target channel's RAG program required a switch to low-beam data within the range of operational concern for wind shear measurements, the indicated paths would reverse; the dedicated weather receiver would accept high-beam data, whereas low-beam signals would enter the wind shear processor via the target channel A/D converters.

When the radar transmits CP signals, the weather-channel receiver is switched to the single RF path from the orthogonal-sense antenna ports. In this mode, it is not currently possible to access high- and low-beam orthogonally polarized signals simultaneously. Unless a new rotary joint is installed, use of the cross-spectral phase method described above would be precluded. However, amplitude comparisons (such as the spectral differencing and autocorrelation-based methods) can be accomplished by switching between the high and low beams on alternate antenna scans.

The radar hardware needed to implement the necessary changes consists therefore of switches, a receiver chain, and A/D converters. Local oscillator signals must be extracted from the exciter chain and suitable microwave plumbing provided.

As part of our field measurement program in 1989, we deployed a real-time signal processing system at the testbed ASR that implemented some of the hazard-detection sequences described in this article. The system uses VME-bus-compatible single-board computers for control and for microburst-detection algorithm processing; high-speed signal processing operations are accomplished in array processor boards. The processors are modular and can be expanded to achieve computational speeds on the order of 100 million floating-point operations per second. The system generates real-time displays of the reflectivity and radial-velocity field out to a range of 30 km, and overlays indicate the location and intensity of automatically detected microburst outflows. Data are archived on magnetic tape.

Summary

Analysis and a field measurement program have demonstrated that a suitably modified ASR can provide high-confidence detection of microbursts associated with surface rain. Since all fatal wind-shear-related air carrier accidents to date have involved wet microbursts, this detection capability represents a significant safety benefit for airports not protected by other systems. At high-priority airports, integration of wind measurements from an ASR with data from TDWR or LLWAS can improve the quality

and/or timeliness of wind shear alarms from the dedicated sensors.

Our current efforts are directed toward a refined understanding of the wind shear detection capability of an ASR, and eventual implementation of this capability in the ATC system. To increase our understanding of wind shear detection, we are simulating ASR signals from low-reflectivity microbursts observed during data collection with the Lincoln Laboratory TDWR test radar in Denver. In addition, data from our current operating site near Kansas City, Mo., are available to quantify the capability of an ASR to measure the strong, operationally significant gust fronts that occur in the midwestern and western United States. Ongoing discussion involving the FAA, Lincoln Laboratory, and supporting research organizations is attempting to clarify how ASR-based wind shear detection will be used. In addition to the possible described retrofit to ASR-9s, wind shear detection will most likely be a built-in capability in the next-generation ASR-10s. In our opinion, the obvious benefits and demonstrated wind shear detection capability justify deployment on both current and future ATC terminal radars.

Acknowledgments

The authors would like to express appreciation to Joe Cullen, Barbara Forman, Mark Meister, Jim Pieronek, Oliver Newell, and Mel Stone at Lincoln Laboratory; to John Anderson and Mark Burzinski of the Meteorology Department at the University of Wisconsin, Madison; and to Wes Johnston, Jay Laseman, and Gene Tellis of General Electric Corporation.

References

1. M.L. Stone and J.R. Anderson, "Advances in Primary-Radar Technology," *Lincoln Laboratory Journal* **2,** 363 (1989).
2. J. Taylor and G. Bronins, "Design of a New Airport Surveillance Radar (ASR-9)," *IEEE Proc.* **73,** 284 (1985).
3. M.E. Weber, "Assessment of ASR-9 Weather Channel Performance: Analysis and Simulation," *Project Report ATC-138,* Lincoln Laboratory (1986), FAA-PM-86-16.
4. T.T. Fujita, "The Downburst," *Research Paper 210, Satellite and Mesometeorology Research Project,* University of Chicago (1985).
5. R.C. Goff, "Some Observations of Thunderstorm Induced Low-Level Wind Variations," *Amer. Inst. of Aeronautics and Astronautics, 9th Fluid and Plasma Dynamics Conf., San Diego, CA, 14–16 July 1976,* AIAA Paper No. 76-388.
6. R.C. Goff, "The Federal Aviation Administration's Low Level Windshear Alert System: A Project Management Perspective," *Preprints, 3rd Intl. Conf. on the Aviation Weather System, Anaheim, CA, 30 Jan.–3 Feb. 1989.*
7. M.W. Merritt, D. Klingle-Wilson, and S.D. Campbell, "Wind Shear Detection with Pencil-Beam Radars," *Lincoln Laboratory Journal* **2,** 483 (1989).
8. J.R. Anderson, "The Measurement of Doppler Wind Fields with Fast Scanning Radars: Signal Processing Techniques," *J. Appl. Meteorol.* **4,** 627 (1987).
9. M.E. Weber, "Ground Clutter Processing for Wind Measurements with Airport Surveillance Radars," *Project Report ATC-143,* Lincoln Laboratory (1987), FAA-PM-87-21.
10. M.E. Weber and W.R. Moser, "A Preliminary Assessment of Thunderstorm Outflow Wind Measurement with Airport Surveillance Radars," *Project Report ATC-140,* Lincoln Laboratory (1987), FAA-PM-86-38.
11. P. Biron and M. Isaminger, "High Resolution Microburst Outflow Depth Data from Huntsville, Alabama and Denver, Colorado," *Project Report ATC-163,* Lincoln Laboratory (1989), in press.
12. D. Atlas, "The Detection of Low-Level Windshear with Airport Surveillance Radar," *3rd Intl. Conf. on the Aviation Weather System, Anaheim, CA, 30 Jan.–3 Feb. 1989.*
13. M.E. Weber and T.A. Noyes, "Low-Altitude Wind Shear Detection with Airport Surveillance Radars: Evaluation of 1987 Field Measurements," *Project Report ATC-159,* Lincoln Laboratory (1988), FAA-PS-88-10.
14. M.E. Weber, "Dual-Beam Autocorrelation Based Wind Estimates from Airport Surveillance Radar Signals," *Project Report ATC-167,* Lincoln Laboratory (1989), FAA-PS-89-5.
15. J. Anderson, "Techniques for the Detection of Microburst Outflows Using Airport Surveillance Radars," *3rd Intl. Conf. on the Aviation Weather System, Anaheim, CA, 30 Jan.–3 Feb. 1989.*
16. R. Gonzalez and P. Wintz, *Digital Image Processing* (Addison-Wesley, Reading, MA, 1987), p. 30.
17. J. Foley and A. Van Dam, *Fundamentals of Interactive Computer Graphics* (Addison-Wesley, Reading, MA, 1983), p. 521
18. M.M. Wolfson, "Characteristics of Microbursts in the Continental United States," *Lincoln Laboratory Journal,* **1,** 49 (1988).

MARK E. WEBER is a staff member in the Air Traffic Surveillance group. He received a B.A. in physics from Washington University in St. Louis and a Ph.D. in physics from Rice University. His areas of research speciality include sonar and Doppler radar signal processing, atmospheric and ocean sound propagation, and thundercloud electrification phenomena. Before coming to Lincoln Laboratory in 1984, Mark held postdoctoral appointments at Rice University and Columbia University, and worked at the U.S. Naval Research Laboratory.

TERRI A. NOYES is a staff member in the Air Traffic Surveillance Group. She received a B.S. in Computer and Information Science, with a second major in mathematics, from the University of Massachusetts at Amherst, where she worked as a research assistant in the Perceptual Robotics Laboratory. She received an M.S. in Computer Science from Rensselaer Polytechnic Institute, where she specialized in two- and three-dimensional image understanding. Before joining Lincoln Laboratory in 1987, Terri worked at the General Electric Corporate Research and Development Center in Schenectady, N.Y.